

# Ultrathin, High-Aspect Ratio, and Free-Standing Magnetic Nanowires by Exfoliation of Ferromagnetic Quasi-One-Dimensional van der Waals Lattices

Yi Qu,<sup>§</sup> Maxx Q. Arguilla,<sup>§</sup> Qiang Zhang, Xin He, and Mircea Dincă\*

**Cite This:** *J. Am. Chem. Soc.* 2021, 143, 19551–19558

**Read Online**

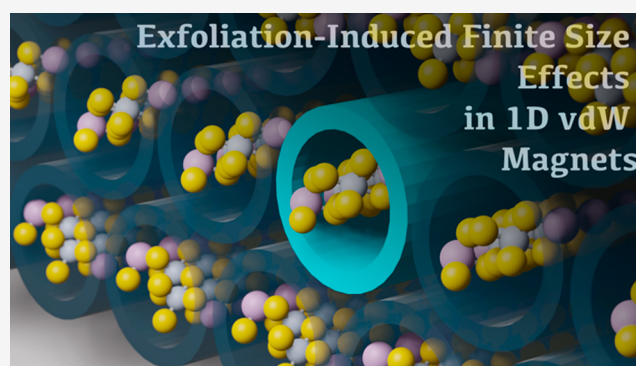
ACCESS |

Metrics & More

Article Recommendations

Supporting Information

**ABSTRACT:** Driven by numerous discoveries of novel physical properties and integration into functional devices, interest in one-dimensional (1D) magnetic nanostructures has grown tremendously. Traditionally, such structures are accessed with bottom-up techniques, but these require increasing sophistication to allow precise control over crystallinity, branching, aspect ratio, and surface termination, especially when approaching the subnanometer regime in magnetic phases. Here, we show that mechanical exfoliation of bulk quasi-one-dimensional crystals, a method similar to those popularized for two-dimensional van der Waals (vdW) lattices, serves as an efficient top-down method to produce ultrathin freestanding nanowires that are both magnetic and semiconducting. We use CrSbSe<sub>3</sub> as a representative quasi-1D vdW crystal with strong magnetocrystalline anisotropy and show that it can be exfoliated into nanowires with an average cross-section of  $10 \pm 2.8$  nm. The CrSbSe<sub>3</sub> nanowires display reduced Curie–Weiss temperature but higher coercivity and remanence than the bulk phase. The methodology developed here for CrSbSe<sub>3</sub>, a representative for a vast class of 1D vdW lattices, serves as a blueprint for investigating confinement effects for 1D materials and accessing functional nanowires that are difficult to produce via traditional bottom-up methods.



## INTRODUCTION

Nanoscale low-dimensional magnetic devices have enabled studies of a vast range of exotic physical phenomena<sup>1–3</sup> such as spin-Peierls transitions in spin chains<sup>4</sup> and superconductivity in spin-ladder systems<sup>5</sup> and have given rise to technologies spanning magnetic refrigeration,<sup>6,7</sup> implantable bioelectronics,<sup>8,9</sup> and data storage devices.<sup>10–14</sup> Many of these technologies benefit from the use of one-dimensional (1D) magnetic nanostructures, which have smaller footprints, greater sensitivity toward external stimuli, and enhanced coercivity enabled by their inherent shape anisotropy.<sup>15</sup> The advantages conferred by nanowires have led to numerous advances in bottom-up synthetic routes, such as vapor- and solution-phase growth,<sup>16–18</sup> electrodeposition,<sup>19–21</sup> and lithographic methods,<sup>22,23</sup> which can yield freestanding magnetic nanowires with well-defined diameters, lengths, compositions, and phase purity. Challenges remain, however, because these traditional bottom-up methods often do not allow for precise control over the long-range nanowire morphologies, and they typically lead to surface passivation and the formation of defects.<sup>24–29</sup> Alternatively, one can employ top-down approaches to isolate wires from bulk crystals, as demonstrated with Mo<sub>6</sub>S<sub>3</sub>I<sub>6</sub>,<sup>30–33</sup> SnIP,<sup>34</sup> and V<sub>2</sub>Se<sub>9</sub>,<sup>35,36</sup> which comprise strong covalently bonded molecular chains connected by van der Waals (vdW)

interchain interactions. This approach has shown great promise because starting from ostensibly more highly ordered and surface defect-free bulk crystals yields nanowires whose structural and physical properties enable potential applications in transistors and photovoltaic devices.<sup>30,37–47</sup> To our knowledge, however, these softer methodologies have not been extended to magnetic vdW phases and, critically, their utility in accessing highly desirable ultrathin magnetic nanowires remains largely unexplored.

Here, we describe a top-down approach to fabricating semiconducting magnetic nanowires from bulk crystals comprising 1D inorganic magnetic chains held together predominantly by vdW interactions. Contrasting with related methods pioneered for instance with the solution stabilization of Li<sub>2</sub>Mo<sub>6</sub>Se<sub>6</sub> highly polar solvents,<sup>48,49</sup> this method is distinct because it does not require cation solvation and produces free-standing nanowires that do not require solution or surface

**Received:** September 10, 2021

**Published:** November 9, 2021



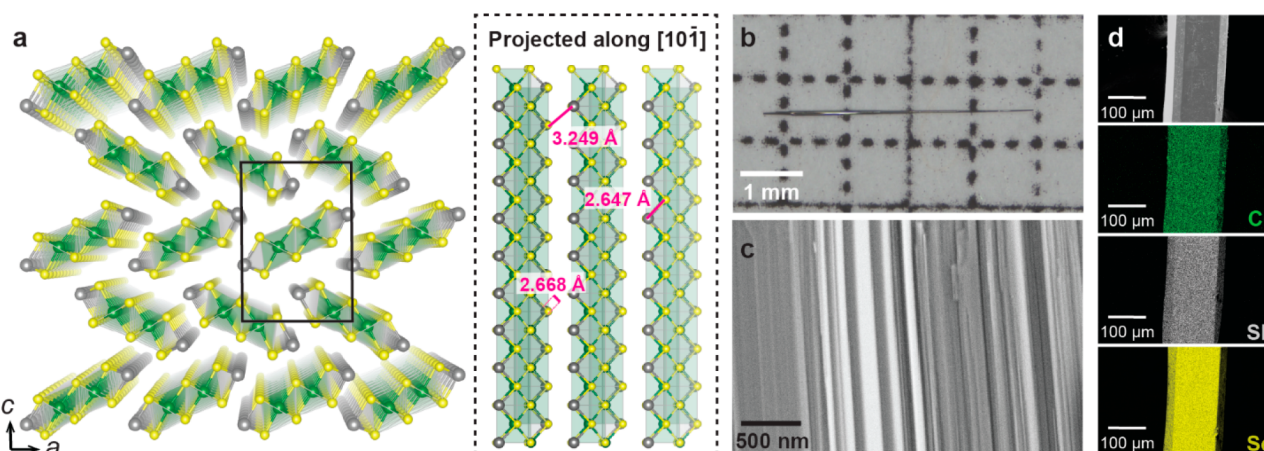


**Figure 1.** Structure and characterization of  $\text{CrSbSe}_3$ . (a) X-ray crystal structure of  $\text{CrSbSe}_3$  at 298 K, with the unit cell outlined in black (left) and the double-rutile chains extending along the  $b$  axis labeled with three relevant Sb–Se distances (right). Green, gray, and yellow spheres represent Cr, Sb, and Se, respectively. (b) A single crystal of flux-grown  $\text{CrSbSe}_3$ . (c) SEM micrograph of an as-synthesized  $\text{CrSbSe}_3$  single crystal after mechanical cleavage. (d) SEM micrograph with the corresponding EDS elemental maps of  $\text{CrSbSe}_3$ .

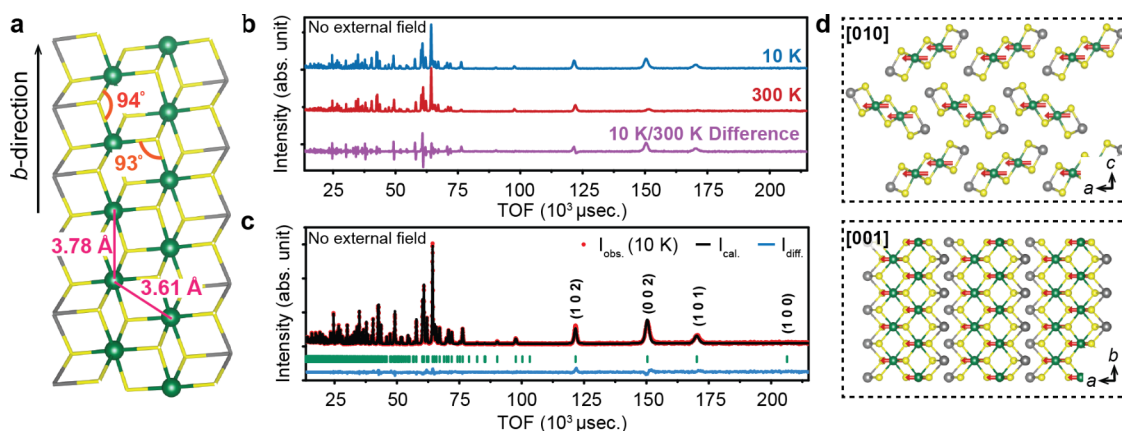


**Figure 2.** Magnetic structure of the  $\text{CrSbSe}_3$  lattice. (a) Comparison of the neutron diffraction profiles at 10 K (ferromagnetic state) and 300 K (paramagnetic state) in the absence of an external magnetic field. (b) Final observed (red dots), fitted (black curve), and difference (blue curve) powder neutron diffractograms of bulk  $\text{CrSbSe}_3$ . Several zone axes of interest are labeled with their respective Miller indices. (c) Refined magnetic structure of  $\text{CrSbSe}_3$  derived from the powder neutron diffraction profile projected along the [010] (top) and [001] (bottom) axes.

stabilization. In fact, the methodology reported here is most closely related to the mechanical exfoliation of 2D vdW phases popularized with graphene and transition metal dichalcogenides. Indeed, although exfoliation is obviously widely used with bulk 2D vdW lattices, including for producing free-standing ultrathin magnetic sheets,<sup>50–57</sup> it has rarely, if ever, been used on bulk 1D vdW magnetic lattices, whose magnetic behavior upon dimensional reduction to the nanowire regime likewise remains poorly understood.

To highlight the potential utility of 1D vdW exfoliation in the production of magnetic nanowires, we chose  $\text{CrSbSe}_3$  as a representative example. Although there are numerous bulk phases that can be described as 1D vdW crystals, exceedingly few show magnetic ordering.<sup>58–62</sup> Featuring weakly associated double-rutile chains of covalently bonded atoms, bulk  $\text{CrSbSe}_3$  exhibits robust ferromagnetic ordering below 71 K.<sup>63,64</sup> The Sb atoms are critical: their lone pairs provide steric repulsion that separate individual  $\text{CrSbSe}_3$  chains and open vdW gaps. We used time-of-flight (TOF) powder neutron diffraction to establish the ferromagnetic ground state and the apparent magnetocrystalline anisotropy of  $\text{CrSbSe}_3$  and show that as-synthesized  $\text{CrSbSe}_3$  crystals can be readily exfoliated into 10

$\pm 2.8$  nm thick nanowires. Importantly, the exfoliated  $\text{CrSbSe}_3$  nanowires are resistant to oxidation under ambient conditions. Exfoliation of the bulk crystals into long and thin nanowires significantly decreases the Curie–Weiss temperature ( $\theta_{\text{CW}}$ ) and simultaneously increases their coercivity and remanence. Exfoliation thus produces a harder ferromagnetic phase than bulk  $\text{CrSbSe}_3$ , as has also been seen upon nanostructuring traditional ferromagnets such as Ni and  $\text{Fe}_2\text{O}_3$ .<sup>65,66</sup> These findings demonstrate that well-established exfoliation methods can be adapted to new classes of functional vdW lattices, particularly for the creation of 1D magnetic nanostructures.

## RESULTS AND DISCUSSION

As reported previously,  $\text{CrSbSe}_3$  crystallizes in the orthorhombic  $Pnma$  space group and features double-rutile chains of covalently bonded atoms extending along the  $b$  axis (Figure 1a).<sup>63,64</sup> The Sb atoms occupying the edge of the double-rutile chains bind three Se atoms in trigonal pyramidal geometry. Owing to the close electronegativity values of Sb and Se, the lone pair on Sb provides steric repulsion and forms a vdW gap with Se orbitals on neighboring chains. Indeed, the nearest neighbor distance between a Sb atom on one chain and a Se

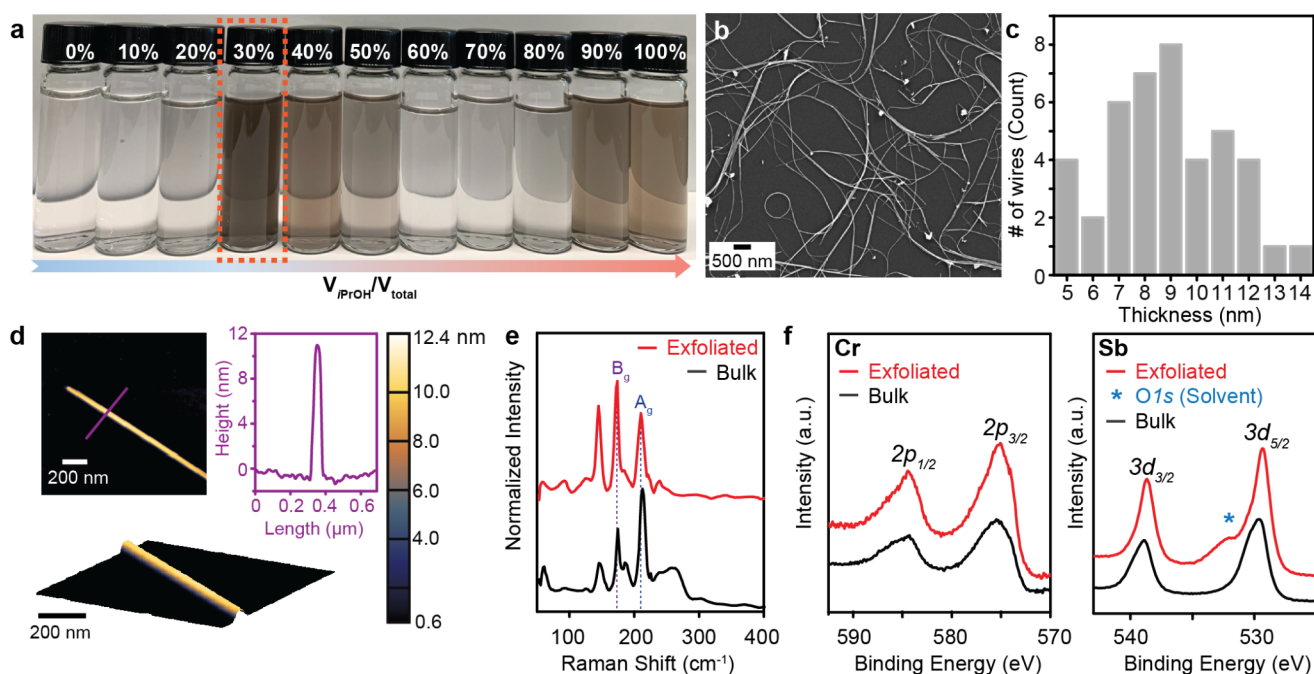


**Figure 3.** Morphology and stability of solution-exfoliated CrSbSe<sub>3</sub> nanowires. (a) CrSbSe<sub>3</sub> dispersions in *i*PrOH/H<sub>2</sub>O solvent mixtures with increasing *i*PrOH volume ratios (% $V_{i\text{PrOH}}/V_{\text{total}}$ ) and decreasing polarity from left to right.  $V_{\text{total}}$  denotes the total volume of *i*PrOH and H<sub>2</sub>O. (b) Representative SEM micrograph of the drop-casted CrSbSe<sub>3</sub> nanowires on 300 nm SiO<sub>2</sub>/Si. (c) Cross-section distributions of CrSbSe<sub>3</sub> nanowires determined by AFM imaging. (d) AFM image of a single CrSbSe<sub>3</sub> nanowire with the corresponding line profile (top) and 3D topographical view (bottom). (e) Micro-Raman spectra of the bulk and exfoliated CrSbSe<sub>3</sub>. The symmetries of the phonon modes corresponding to directions perpendicular ( $A_g$ ) and parallel ( $B_g$ ) to the crystal long axis are labeled in blue and purple, respectively. (f) XPS spectra of the Cr 2p and the Sb 3d of both bulk crystals and exfoliated nanowires of CrSbSe<sub>3</sub>. In the Sb 3d spectrum, the peak marked by an asterisk corresponds to the O 1s contribution from the exfoliation solvent.

atom on an adjacent chain, 3.2494(9) Å, is much longer than the Sb–Se bond distances within a chain: 2.6473(8) Å and 2.6679(11) Å (Figure 1a, Table S4). Bulk CrSbSe<sub>3</sub> is grown either by typical solid state melt synthesis, which yields polycrystalline powders, or by flux growth, which yields needle-like millimeter-sized single crystals with fibrous morphology, a macroscopic indication of the quasi-1D vdW nature of the crystals (Figure 1b,c; see section I in Supporting Information for synthesis details). Elemental mapping by energy-dispersive X-ray spectroscopy (EDS) confirmed the homogeneous distribution of Cr, Sb, and Se throughout the crystals (Figure 1d).

We used TOF powder neutron diffraction to determine the magnetic structure and correlate structural parameters in CrSbSe<sub>3</sub> with its established bulk ferromagnetic behavior. It had been shown that the ferromagnetic transition temperature ( $T_C$ ) of bulk CrSbSe<sub>3</sub> is at approximately 71 K. As such, we refined neutron diffraction data above and below  $T_C$ . Significantly, data collected at 10 K displayed increased intensity for several Bragg peaks at the high TOF (>100 000  $\mu\text{s}$ ) or  $d$ -spacing region (Figure 2a). Indexing and refinement of this data revealed that the magnetic unit cell has the same parameters as the crystallographic unit cell (Figure 2b, Tables S2 and S3). Rietveld refinement of the neutron diffraction patterns revealed ferromagnetic order with spin moments aligned along the  $a$  axis (Figure 2c). Because magnetic neutron scattering is sensitive only to the magnetic moment components that are perpendicular to the scattering vector, the absence of the magnetic (100) peak indicates perfect alignment of the ferromagnetically ordered moments along the  $a$  axis, without spin canting. These data confirm the

magnetocrystalline anisotropy and the magnetic easy axis, previously suggested solely on the basis of magnetic susceptibility measurements of oriented crystals.<sup>63</sup> Similarly, the neutron-diffraction-derived magnetic moment of 3.06(7)  $\mu_B/\text{Cr}$  is consistent with the ground spin state of  $S = 3/2$  for Cr(III), determined from magnetization data.

With evidence in hand that CrSbSe<sub>3</sub> presents as a quasi-1D vdW crystal that shows both magnetic ordering and significant anisotropy, we sought to investigate changes to these properties upon isolating nanowires from the bulk. To do so, we employed a solution technique pervasive in 2D vdW materials that involves systematic tuning of polarity and dispersity of solvent mixtures to optimize exfoliation.<sup>67–70</sup> To this end, the isopropanol (*i*PrOH)–water mixture covers a wide range of both dispersive and polar parameters and was also used here.<sup>70,71</sup> For CrSbSe<sub>3</sub>, we found that a volumetric 30:70 *i*PrOH/water mixture yields the highest concentration of dispersed CrSbSe<sub>3</sub> nanowires (Figure 3a, Table S5). Although exfoliation of bulk CrSbSe<sub>3</sub> powder in 100% *i*PrOH also gives a somewhat even more concentrated dispersion, it leads to isotropic nanoparticles of CrSbSe<sub>3</sub> rather than nanowires (Figure S4). Subjecting the suspended CrSbSe<sub>3</sub> nanowires to liquid cascade centrifugation (see section I in Supporting Information for exfoliation details) yields abundant nanowires with lengths exceeding 1  $\mu\text{m}$  (Figures 3b and S1). Measurement of 70 individual randomly oriented nanowires using atomic force microscopy (AFM) gave an average cross-section of  $10 \pm 2.8$  nm (Figures 3c and S2). Thus, the exfoliation–centrifugation method is particularly efficient at producing ultrathin and long wires with a narrow cross-sectional distribution. Indeed, three-dimensional AFM topographical

view of single nanowires revealed uniform thickness along the length of the nanowire, with no tapering, branching, or kinking that is often seen in nanowires grown by bottom-up methods (Figure 3d bottom). Furthermore, nanowires produced by our method are smooth, with surface roughness of  $\pm 0.2$  nm over 1  $\mu\text{m}$ , further highlighting the absence of morphological distortions, discontinuities, or cracks along the nanowire surface (Figure S3). This successful exfoliation process demonstrates that concepts and techniques in traditional top-down exfoliation in 2D vdW materials can be extended and translated to magnetic vdW materials with lower dimensionalities.

Raman spectroscopy and X-ray photoelectron spectroscopy (XPS) confirmed the phase identity, crystallinity, and surface stability of the exfoliated CrSbSe<sub>3</sub> nanowires. Because phonon modes are directly correlated to the structural identity and inherent crystallinity of a material, we probed the evolution of these modes in CrSbSe<sub>3</sub> upon its exfoliation from bulk into nanowires. As shown in Figure 3e (see also section 4 in Supporting Information), all Raman modes present in bulk CrSbSe<sub>3</sub> are also found in exfoliated nanowires, including the most prominent bands at 212.8 and 174.4  $\text{cm}^{-1}$ , whose narrow full-width-at-half-maximum values of 10.0 and 6.3  $\text{cm}^{-1}$ , respectively, remain nearly unchanged and indicate a high degree of crystallinity. We attribute lower energy shifts of approximately 2  $\text{cm}^{-1}$  to phonon confinement effects as the lattice is reduced from bulk to nanowires.<sup>72</sup> XPS of CrSbSe<sub>3</sub> single crystals and exfoliated nanowires, shown in Figure 3f, revealed two energy bands for Cr, at 575.2 eV ( $2p_{3/2}$ ) and 584.6 eV ( $2p_{1/2}$ ), which agree well with the reported binding energy of Cr 2p in similar coordination environments.<sup>73</sup> The broad nonsymmetric peak shape of the Cr 2p peaks can be attributed to multiplet splitting, which is common for Cr(III) compounds (see Figure S6 for detailed peak fitting).<sup>74</sup> Similarly, the Sb 3d spectra of bulk crystals and exfoliated nanowires both show two bands at 529.3 eV ( $3d_{5/2}$ ) and 538.8 eV ( $3d_{3/2}$ ), in good agreement with literature values for Sb (see Figure S7 for detailed peak fitting).<sup>75</sup> Notably, there are no signs of oxidation upon exfoliation, as evidenced by the absence of higher binding energy peaks in both the Cr 2p and the Sb 3d regions (see Se 3d region in Figure S8).

Exfoliating bulk crystals into nanowires allows systematic studies for understanding the evolution of magnetic properties of CrSbSe<sub>3</sub> upon nanosizing. We first confirmed the magnetic properties of bulk CrSbSe<sub>3</sub> by susceptibility measurements from 2 to 300 K under an applied field of 1 kOe. A linear fit of these data in the high temperature region gives an effective moment of 4.2  $\mu_{\text{B}}/\text{Cr}$ , in agreement with the spin-only value expected for Cr(III) (3.9  $\mu_{\text{B}}$ ). Fitting these data to the Curie–Weiss law gives  $\theta_{\text{CW}} \sim 133$  K, indicating ferromagnetic coupling between the Cr<sup>3+</sup> centers, with  $T_{\text{C}}$  of around 70 K (see fitting details in Table S7). The field-dependent magnetization curve at 2 K collected at fields up to 80 kOe saturates at 3  $\mu_{\text{B}}/\text{Cr}$ , further confirming both the phase purity and ferromagnetic ordering of the Cr<sup>3+</sup> spins in the bulk CrSbSe<sub>3</sub> lattice (Figure 4a). Close inspection of the magnetic hysteresis loop indicates that both the coercivity,  $H_{\text{c}}$ , and the remanence are very low ( $H_{\text{c}} = 140$  Oe), in agreement with previous reports classifying bulk CrSbSe<sub>3</sub> as a soft ferromagnet.<sup>63,64</sup>

Generally, the magnetization behavior of nanostructures tends to minimize the total free energy in terms of exchange energy, Zeeman energy, magnetoelastic energy, and anisotropy

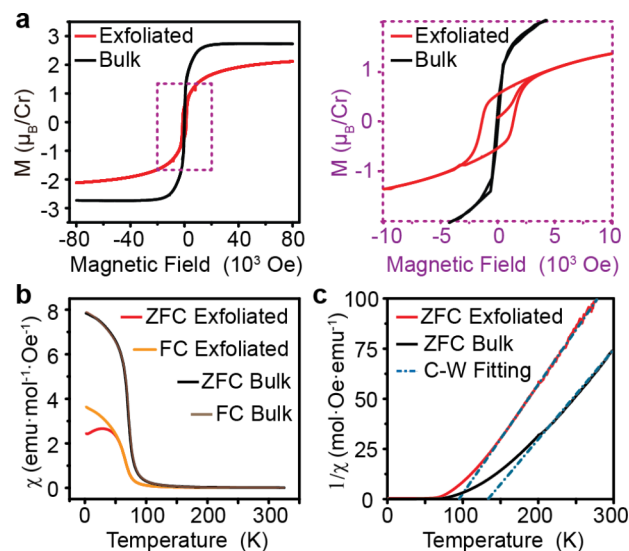


**Figure 4.** Magnetic properties of bulk polycrystalline powder and exfoliated nanowires of CrSbSe<sub>3</sub>. (a) Comparison of the  $M$ – $H$  data for bulk and exfoliated nanowires of CrSbSe<sub>3</sub> at 2 K. (b) Temperature dependent field-cooled (FC) and zero-field-cooled (ZFC) molar magnetic susceptibility curves of bulk and exfoliated CrSbSe<sub>3</sub> under an applied field of 1 kOe. (c) Curie–Weiss fits of the temperature-dependent inverse susceptibilities for bulk and exfoliated CrSbSe<sub>3</sub>.

energy. Among these, the variation of the anisotropy term with particle shape has been experimentally and theoretically investigated extensively<sup>20,76,77</sup> and has been found to significantly influence fundamental magnetic properties including the coercivity, remanence, saturation magnetization, easy axis, and magnetic reversal process.<sup>20,77,78</sup> Naturally, particle size also affects physical properties, especially when reaching the nanometer regime.<sup>79</sup> In magnetism, these finite-size effects are evident, for instance, when the particle size reaches that of the excitation wavelength of magnons, the domain wall width, or the spin–spin correlation length. Given the significantly altered morphology and particle size upon exfoliation, it is therefore reasonable to expect that nanowires of CrSbSe<sub>3</sub> should show different magnetic properties from the bulk.

Directly probing the magnetic properties of a single nanowire by magnetic force microscopy or magnetic–optical methods such as Kerr microscopy is challenging due to the low magnetic ordering temperature of CrSbSe<sub>3</sub> and the extreme thinness of the exfoliated nanowires that is well below the optical diffraction limit. An alternative method, demonstrated previously for exfoliated 2D hematite crystals, involves collecting the exfoliated particles and interpreting their collective magnetic properties.<sup>66</sup> Here, we filtered the final supernatant after the liquid cascade centrifugation and collected about 1 mg of exfoliated CrSbSe<sub>3</sub> nanowires. The shape of the magnetization curve for these nanowires (Figure 4a) suggests that the long-range ferromagnetic ordering present in bulk CrSbSe<sub>3</sub> persists upon exfoliation. However, the hysteresis loop demonstrates that the coercivity is significantly enhanced by as much as 1 order of magnitude, from  $H_{\text{c}} = 0.14$  kOe in the bulk to  $H_{\text{c}} = 1.5$  kOe in the exfoliated nanowires, and that the remanence increases from 0.2  $\mu_{\text{B}}/\text{Cr}$  in the bulk to 0.5  $\mu_{\text{B}}/\text{Cr}$  in the exfoliated nanowires. Notably, these results suggest that upon exfoliation into ultrathin nanowires, CrSbSe<sub>3</sub> transitions from a soft to a hard ferromagnet. Similar transitions have been observed for other

low-dimensional magnetic systems and are often assigned to increasing anisotropy.<sup>80–84</sup> In bulk CrSbSe<sub>3</sub>, although the spins prefer to align along the *a* axis, the magnetocrystalline anisotropy is relatively weak, as manifested by the low coercivity and low remanence. However, exfoliation into nanowires greatly changes the aspect ratio whereby the wire dimension along the crystallographic *b* direction is much longer than along *a* and *c*, giving rise to strong shape anisotropy. Consequently, the anisotropy energy increases, which imposes a greater barrier to spin flipping and induces a greater hysteresis.

Further understanding of the evolution of magnetic properties upon exfoliation came from analyzing the temperature-dependent magnetic susceptibility from 2 to 300 K under an external field of 1 kOe. The zero-field-cooled (ZFC) and field-cooled (FC) magnetization curves bifurcate at low temperatures, consistent with the expected behavior of hard magnets (Figure 4b).<sup>85</sup> The susceptibility data above 140 K can be fitted to the Curie–Weiss law to give a Curie constant of 3.9  $\mu_B$ /Cr and  $\theta_{CW}$  of approximately 95 K. This  $\theta_{CW}$  is 38 K lower than the value for the bulk crystal (Figure 4c, Table S7) and can be ascribed to finite-size effects: in bulk CrSbSe<sub>3</sub>, which is a 3D ferromagnet, the spin–spin correlation length  $\xi$  is expected to increase with temperature and diverge at the ordering temperature.<sup>86</sup> Upon exfoliation, where the dimensions along the crystallographic *a* and *c* directions become significantly smaller, the growth of the correlation length with temperature is constrained by the wire diameter *d*, resulting in a reduced  $\theta_{CW}$ . Although similar finite-size effects have been established both experimentally and theoretically in 2D thin films as well as zero-dimensional nanoparticles,<sup>79,87–90</sup> they are much less investigated in 1D or quasi-1D nanowires, with several theoretical and experimental reports nevertheless showing strong size dependence of  $\theta_{CW}$ .<sup>91</sup>

## CONCLUSIONS

The foregoing results demonstrate that solution exfoliation is an efficient technique for accessing ultrathin ferromagnetic nanowires with high aspect ratio from bulk crystals of 1D vdW-connected lattices. As proof-of-principle, we showed that CrSbSe<sub>3</sub>, a bulk ferromagnet made from vdW-connected 1D chains, serves as a good precursor for obtaining air-stable, free-standing nanowires that show increased coercivity and remanence compared to the bulk. These results provide a blueprint for additional studies with other bulk 1D vdW crystals. They further motivate studies aimed at understanding how magnetic interactions in bulk crystals evolve upon nanostructuring.

## ASSOCIATED CONTENT

### Supporting Information

The Supporting Information is available free of charge at <https://pubs.acs.org/doi/10.1021/jacs.1c09607>.

Additional experimental details and characterization data (PDF)

## AUTHOR INFORMATION

### Corresponding Author

Mircea Dincă – Department of Chemistry, Massachusetts Institute of Technology, Cambridge, Massachusetts 02139, United States; [orcid.org/0000-0002-1262-1264](https://orcid.org/0000-0002-1262-1264); Email: [mdinca@mit.edu](mailto:mdinca@mit.edu)

## Authors

Yi Qu – Department of Chemistry, Massachusetts Institute of Technology, Cambridge, Massachusetts 02139, United States

Maxx Q. Arguilla – Department of Chemistry, Massachusetts Institute of Technology, Cambridge, Massachusetts 02139, United States

Qiang Zhang – Neutron Scattering Division, Oak Ridge National Laboratory, Oak Ridge, Tennessee 37831, United States

Xin He – Department of Chemistry, Massachusetts Institute of Technology, Cambridge, Massachusetts 02139, United States; [orcid.org/0000-0001-8461-8868](https://orcid.org/0000-0001-8461-8868)

Complete contact information is available at: <https://pubs.acs.org/10.1021/jacs.1c09607>

## Author Contributions

<sup>§</sup>Y.Q. and M.Q.A. contributed equally.

## Notes

The authors declare no competing financial interest.

## ACKNOWLEDGMENTS

The experimental work was supported by the Army Research Office (Award W911NF-21-1-0124). Neutron experiments used resources at the Spallation Neutron Source, a DOE Office of Science User Facility operated by the Oak Ridge National Laboratory. Part of the characterization was performed at the Harvard Center for Nanoscale Systems (CNS), a member of the National Nanotechnology Infrastructure Network (NNIN), which is supported by the National Science Foundation (Award ECS-0335765).

## REFERENCES

- (1) Dejongh, L. J.; Miedema, A. R. Experiments on Simple Magnetic Model Systems. *Adv. Phys.* **1974**, *23* (1), 1–260.
- (2) Steiner, M.; Villain, J.; Windsor, C. G. Theoretical and Experimental Studies on One-Dimensional Magnetic Systems. *Adv. Phys.* **1976**, *25* (2), 87–209.
- (3) Li, M. Y. M.; Claire, F. J.; Solomos, M. A.; Tenney, S. M.; Ivanov, S. A.; Siegler, M. A.; Kempa, T. J. Molecular Chains of Coordinated Dimolybdenum Isonicotinate Paddlewheel Clusters. *RSC Adv.* **2019**, *9* (29), 16492–16495.
- (4) Bray, J. W.; Hart, H. R.; Interrante, L. V.; Jacobs, I. S.; Kasper, J. S.; Watkins, G. D.; Wee, S. H.; Bonner, J. C. Observation of a Spin-Peierls Transition in a Heisenberg Antiferromagnetic Linear-Chain System. *Phys. Rev. Lett.* **1975**, *35* (11), 744–747.
- (5) Maekawa, S. Superconductivity in Spin Ladders. *Science* **1996**, *273* (5281), 1515–1515.
- (6) Gschneidner, K. A.; Pecharsky, V. K.; Tsokol, A. O. Recent Developments in Magnetocaloric Materials. *Rep. Prog. Phys.* **2005**, *68* (6), 1479–1539.
- (7) Gutfleisch, O.; Willard, M. A.; Bruck, E.; Chen, C. H.; Sankar, S. G.; Liu, J. P. Magnetic Materials and Devices for the 21st Century: Stronger, Lighter, and More Energy Efficient. *Adv. Mater.* **2011**, *23* (7), 821–842.
- (8) Yuan, J. Y.; Xu, Y. Y.; Muller, A. H. E. One-dimensional Magnetic Inorganic-organic Hybrid Nanomaterials. *Chem. Soc. Rev.* **2011**, *40* (2), 640–655.
- (9) Long, Y. Z.; Yu, M.; Sun, B.; Gu, C. Z.; Fan, Z. Y. Recent Advances in Large-scale Assembly of Semiconducting Inorganic Nanowires and Nanofibers for Electronics, Sensors and Photovoltaics. *Chem. Soc. Rev.* **2012**, *41* (12), 4560–4580.
- (10) Caretta, L.; Mann, M.; Buttner, F.; Ueda, K.; Pfau, B.; Gunther, C. M.; Hessing, P.; Churikova, A.; Klose, C.; Schneider, M.; Engel, D.; Marcus, C.; Bono, D.; Bagschik, K.; Eisebitt, S.; Beach, G. S. D. Fast

Current-driven Domain Walls and Small Skyrmions in a Compensated Ferrimagnet. *Nat. Nanotechnol.* **2018**, *13* (12), 1154–1160.

(11) Sun, S. H.; Murray, C. B.; Weller, D.; Folks, L.; Moser, A. Monodisperse FePt Nanoparticles and Ferromagnetic FePt Nanocrystal Superlattices. *Science* **2000**, *287* (5460), 1989–1992.

(12) Allwood, D. A.; Xiong, G.; Faulkner, C. C.; Atkinson, D.; Petit, D.; Cowburn, R. P. Magnetic Domain-wall Logic. *Science* **2005**, *309* (5741), 1688–1692.

(13) Zhou, B. H.; Rinehart, J. D. A Size Threshold for Enhanced Magnetoresistance in Colloidally Prepared  $\text{CoFe}_2\text{O}_4$  Nanoparticle Solids. *ACS Cent. Sci.* **2018**, *4* (9), 1222–1227.

(14) Zhou, B. H.; Rinehart, J. D. Pseudo Spin Valve Behavior in Colloidally Prepared Nanoparticle Films. *ACS Appl. Electron. Mater.* **2019**, *1* (7), 1065–1069.

(15) Stano, M.; Fruchart, O.; Bruck, E. Magnetic Nanowires and Nanotubes. In *Handbook of Magnetic Materials*; Elsevier: Amsterdam, 2018; Vol. 27, Chapter 3, pp 155–267.

(16) Dasgupta, N. P.; Sun, J. W.; Liu, C.; Brittan, S.; Andrews, S. C.; Lim, J.; Gao, H. W.; Yan, R. X.; Yang, P. D. 25th Anniversary Article: Semiconductor Nanowires Synthesis, Characterization, and Applications. *Adv. Mater.* **2014**, *26* (14), 2137–2184.

(17) Duan, X. F.; Lieber, C. M. General Synthesis of Compound Semiconductor Nanowires. *Adv. Mater.* **2000**, *12* (4), 298–302.

(18) Chowdhury, T.; Sadler, E. C.; Kempa, T. J. Progress and Prospects in Transition-Metal Dichalcogenide Research Beyond 2D. *Chem. Rev.* **2020**, *120* (22), 12563–12591.

(19) Cao, G. Z.; Liu, D. W. Template-based synthesis of nanorod, nanowire, and nanotube arrays. *Adv. Colloid Interface Sci.* **2008**, *136* (1–2), 45–64.

(20) Sellmyer, D. J.; Zheng, M.; Skomski, R. Magnetism of Fe, Co and Ni Nanowires in Self-assembled Arrays. *J. Phys.: Condens. Matter* **2001**, *13* (25), R433–R460.

(21) Kohli, S.; McCurdy, P. R.; Johnson, D. C.; Das, J.; Prieto, A. L.; Rithner, C. D.; Fisher, E. R. Template-Assisted Chemical Vapor Deposited Spinel Ferrite Nanotubes. *J. Phys. Chem. C* **2010**, *114* (46), 19557–19561.

(22) Ross, C. A.; Smith, H. I.; Savas, T.; Schattenburg, M.; Farhoud, M.; Hwang, M.; Walsh, M.; Abraham, M. C.; Ram, R. J. Fabrication of Patterned Media for High Density Magnetic Storage. *J. Vac. Sci. Technol., B: Microelectron. Process. Phenom.* **1999**, *17* (6), 3168–3176.

(23) Gambardella, P.; Dallmeyer, A.; Maiti, K.; Malagoli, M. C.; Eberhardt, W.; Kern, K.; Carbone, C. Ferromagnetism in One-dimensional Monatomic Metal Chains. *Nature* **2002**, *416* (6878), 301–304.

(24) Huang, F.; Kief, M. T.; Mankey, G. J.; Willis, R. F. Magnetism in the Few-Monolayers Limit - a Surface Magneto-optic Kerr-Effect Study of the Magnetic-Behavior of Ultrathin Films of Co, Ni, and Co-Ni Alloys on Cu(100) and Cu(111). *Phys. Rev. B: Condens. Matter Mater. Phys.* **1994**, *49* (6), 3962–3971.

(25) Kim, T.; Chamberlin, R. V.; Bird, J. P. Large Magnetoresistance of Nickel-Silicide Nanowires: Non-Equilibrium Heating of Magnetically-Coupled Dangling Bonds. *Nano Lett.* **2013**, *13* (3), 1106–1110.

(26) Seo, K.; Varadwaj, K. S. K.; Mohanty, P.; Lee, S.; Jo, Y.; Jung, M. H.; Kim, J.; Kim, B. Magnetic properties of single-crystalline CoSI nanowires. *Nano Lett.* **2007**, *7* (5), 1240–1245.

(27) Hung, S. W.; Wang, T. T. J.; Chu, L. W.; Chen, L. J. Orientation-Dependent Room-Temperature Ferromagnetism of FeSi Nanowires and Applications in Nonvolatile Memory Devices. *J. Phys. Chem. C* **2011**, *115* (31), 15592–15597.

(28) Tanase, M.; Silevitch, D. M.; Hultgren, A.; Bauer, L. A.; Searson, P. C.; Meyer, G. J.; Reich, D. H. Magnetic Trapping and Self-assembly of Multicomponent Nanowires. *J. Appl. Phys.* **2002**, *91* (10), 8549–8551.

(29) Jorritsma, J.; Mydosh, J. A. Temperature-dependent Magnetic Anisotropy in Ni Nanowires. *J. Appl. Phys.* **1998**, *84* (2), 901–906.

(30) Topolovsek, P.; Gadermaier, C.; Vengust, D.; Strojnik, M.; Strle, J.; Mihailovic, D. Unlocking the Functional Properties in One-Dimensional MoSI Cluster Polymers by Doping and Photoinduced Charge Transfer. *Nano Lett.* **2015**, *15* (2), 813–818.

(31) Celic, N.; Pavlica, E.; Borovsak, M.; Strle, J.; Buh, J.; Zavanik, J.; Bratina, G.; Denk, P.; Scharber, M.; Sariciftci, N. S.; Mihailovic, D. Factors Determining Large Observed Increases in Power Conversion Efficiency of P3HT:PCBM Solar Cells Embedded With  $\text{Mo}_6\text{S}_9\text{I}_x$  Nanowires. *Synth. Met.* **2016**, *212*, 105–112.

(32) Chae, S.; Oh, S.; Choi, K. H.; Jeon, J.; Liu, Z. X.; Wang, C.; Lim, C.; Dong, X.; Woo, C.; Asghar, G.; Chang, J.; Nurunnabi, M.; Kang, J.; Song, S. Y.; Yu, H. K.; Choi, J. Y. Aqueous Dispersion of One-Dimensional van der Waals Material  $\text{Mo}_6\text{S}_3\text{I}_6$  with the Charge Type of the Hydrophobic Dispersant Tail. *ACS Appl. Bio. Mater.* **2020**, *3* (7), 3992–3998.

(33) Lin, H.; Cheng, H. M.; Liu, L.; Zhu, Z. W.; Shao, Y. H.; Papakonstantinou, P.; Mihailovic, D.; Li, M. X. Thionin Attached to a Gold Electrode Modified with Self-assembly of  $\text{Mo}_6\text{S}_9\text{I}_x$  Nanowires for Amplified Electrochemical Detection of Natural DNA. *Biosens. Bioelectron.* **2011**, *26* (5), 1866–1870.

(34) Pfister, D.; Schafer, K.; Ott, C.; Gerke, B.; Pottgen, R.; Janka, O.; Baumgartner, M.; Efimova, A.; Hohmann, A.; Schmidt, P.; Venkatachalam, S.; van Wullen, L.; Schurmann, U.; Kienle, L.; Duppel, V.; Parzinger, E.; Miller, B.; Becker, J.; Holleitner, A.; Wehrich, R.; Nilges, T. Inorganic Double Helices in Semiconducting SnIP. *Adv. Mater.* **2016**, *28* (44), 9783–9791.

(35) Chae, S.; Siddiq, A. J.; Kim, B. J.; Oh, S.; Choi, K. H.; Lee, K. H.; Kim, H. Y.; Yu, H. K.; Choi, J. Y. Isolation of Inorganic Molecular Chains from Rod-like Bulk  $\text{V}_2\text{Se}_5$  Crystal by Liquid Exfoliation. *RSC Adv.* **2018**, *8* (62), 35348–35352.

(36) Lee, W. G.; Sung, D.; Lee, J.; Chung, Y. K.; Kim, B. J.; Choi, K. H.; Lee, S. H.; Jeong, B. J.; Choi, J. Y.; Huh, J. Tuning the Electronic Properties of Highly Anisotropic 2D Dangling-bond-free Sheets from 1D  $\text{V}_2\text{Se}_5$  Chain Structures. *Nanotechnology* **2021**, *32* (9), 095203.

(37) Ploscaru, M. I.; Kokalj, S. J.; Uplaznik, M.; Vengust, D.; Turk, D.; Mrzel, A.; Mihailovic, D.  $\text{Mo}_6\text{S}_9\text{I}_x$  Nanowire Recognitive Molecular-scale Connectivity. *Nano Lett.* **2007**, *7* (6), 1445–1448.

(38) Vrbancic, D.; Pejovnik, S.; Mihailovic, D.; Kutnjak, Z. Electrical Conductivity of  $\text{Mo}_6\text{S}_3\text{I}_6$  and  $\text{Mo}_6\text{S}_{4.5}\text{I}_{4.5}$  Nanowires. *J. Eur. Ceram. Soc.* **2007**, *27* (2–3), 975–978.

(39) Andzane, J.; Prikulis, J.; Dvorsek, D.; Mihailovic, D.; Erts, D. Two-terminal Nanoelectromechanical Bistable Switches Based On Molybdenum-sulfur-iodine Molecular Wire Bundles. *Nanotechnology* **2010**, *21* (12), 125706.

(40) Uplaznik, M.; Bercic, B.; Remskar, M.; Mihailovic, D. Quantum Charge Transport in  $\text{Mo}_6\text{S}_3\text{I}_6$  Molecular Wire Circuits. *Phys. Rev. B: Condens. Matter Mater. Phys.* **2009**, *80* (8), 085402.

(41) Strle, J.; Vengust, D.; Mihailovic, D. Inorganic Molecular-Scale MoSI Nanowire-Gold Nanoparticle Networks Exhibit Self-Organized Critical Self-Assembly. *Nano Lett.* **2009**, *9* (3), 1091–1095.

(42) Chae, S.; Oh, S.; Choi, K. H.; Lee, J. W.; Jeon, J.; Liu, Z. X.; Wang, C.; Woo, C.; Shi, L. Y.; Kang, J.; Song, S. Y.; Kim, S. J.; Lee, J. H.; Yu, H. K.; Choi, J. Y. Aqueous Dispersion of 1D van der Waals  $\text{Mo}_6\text{S}_3\text{I}_6$  Crystal Using Biocompatible Tri-block Copolymer. *Ceram. Int.* **2021**, *47* (9), 11935–11941.

(43) Lee, J. W.; Chae, S.; Oh, S.; Kim, S. H.; Choi, K. H.; Meeseepong, M.; Chang, J.; Kim, N.; Kim, Y. H.; Lee, N. E.; Lee, J. H.; Choi, J. Y. Single-Chain Atomic Crystals as Extracellular Matrix-Mimicking Material with Exceptional Biocompatibility and Bio-activity. *Nano Lett.* **2018**, *18* (12), 7619–7627.

(44) Itzhaik, Y.; Niitsoo, O.; Page, M.; Hodes, G.  $\text{Sb}_2\text{S}_3$ -Sensitized Nanoporous  $\text{TiO}_2$  Solar Cells. *J. Phys. Chem. C* **2009**, *113* (11), 4254–4256.

(45) Majkic, A.; Gadermaier, C.; Celic, N.; Topolovsek, P.; Bratina, G.; Mihailovic, D.  $\text{Mo}_6\text{S}_9\text{I}_x$  Nanowires as Additives for Enhanced organic Solar Cell performance. *Sol. Energy Mater. Sol. Cells* **2014**, *127*, 63–66.

(46) Webber, D. H.; Brutchey, R. L. Alkahest for  $\text{V}_2\text{VI}_3$  Chalcogenides: Dissolution of Nine Bulk Semiconductors in a Diamine-Dithiol Solvent Mixture. *J. Am. Chem. Soc.* **2013**, *135* (42), 15722–15725.

(47) Webber, D. H.; Buckley, J. J.; Antunez, P. D.; Brutchey, R. L. Facile Dissolution of Selenium and Tellurium in a Thiol-amine

Solvent Mixture Under Ambient Conditions. *Chem. Sci.* **2014**, *5* (6), 2498–2502.

(48) Sayettat, J.; Bull, L. M.; Jobic, S.; Gabriel, J. C. P.; Fourmigue, M.; Batail, P.; Brec, R.; Inglebert, R. L.; Sourisseau, C. Behaviour of the One-dimensional, Inorganic Polymer  $^{100}[\text{MPS}_4]^-$  Anions (M = Ni, Pd) in Organic Solutions. *J. Mater. Chem.* **1999**, *9* (1), 143–153.

(49) Tarascon, J. M.; Disalvo, F. J.; Chen, C. H.; Carroll, P. J.; Walsh, M.; Rupp, L. First Example of Monodispersed  $(\text{Mo}_3\text{Se}_3)^{100}$  Clusters. *J. Solid State Chem.* **1985**, *58* (3), 290–300.

(50) Gong, C.; Li, L.; Li, Z. L.; Ji, H. W.; Stern, A.; Xia, Y.; Cao, T.; Bao, W.; Wang, C. Z.; Wang, Y. A.; Qiu, Z. Q.; Cava, R. J.; Louie, S. G.; Xia, J.; Zhang, X. Discovery of Intrinsic Ferromagnetism in Two-dimensional van der Waals Crystals. *Nature* **2017**, *546* (7657), 265–269.

(51) Huang, B.; Clark, G.; Navarro-Moratalla, E.; Klein, D. R.; Cheng, R.; Seyler, K. L.; Zhong, D.; Schmidgall, E.; McGuire, M. A.; Cobden, D. H.; Yao, W.; Xiao, D.; Jarillo-Herrero, P.; Xu, X. D. Layer-dependent Ferromagnetism in a van der Waals Crystal Down to the Monolayer Limit. *Nature* **2017**, *546* (7657), 270–273.

(52) Burch, K. S.; Mandrus, D.; Park, J. G. Magnetism in Two-dimensional van der Waals Materials. *Nature* **2018**, *563* (7729), 47–52.

(53) O'Hara, D. J.; Zhu, T. C.; Trout, A. H.; Ahmed, A. S.; Luo, Y. K.; Lee, C. H.; Brenner, M. R.; Rajan, S.; Gupta, J. A.; McComb, D. W.; Kawakami, R. K. Room Temperature Intrinsic Ferromagnetism in Epitaxial Manganese Selenide Films in the Monolayer Limit. *Nano Lett.* **2018**, *18* (5), 3125–3131.

(54) Bonilla, M.; Kolekar, S.; Ma, Y. J.; Diaz, H. C.; Kalappattil, V.; Das, R.; Eggers, T.; Gutierrez, H. R.; Phan, M. H.; Batzill, M. Strong Room-temperature Ferromagnetism in  $\text{VSe}_2$  Monolayers on van der Waals Substrates. *Nat. Nanotechnol.* **2018**, *13* (4), 289–293.

(55) Lee, J. U.; Lee, S.; Ryoo, J. H.; Kang, S.; Kim, T. Y.; Kim, P.; Park, C. H.; Park, J. G.; Cheong, H. Ising-Type Magnetic Ordering in Atomically Thin  $\text{FeP}_3$ . *Nano Lett.* **2016**, *16* (12), 7433–7438.

(56) Song, X. Y.; Yuan, F.; Schoop, L. M. The Properties and Prospects of Chemically Exfoliated Nanosheets for Quantum Materials in Two Dimensions. *Appl. Phys. Rev.* **2021**, *8* (1), 011312.

(57) Song, X. Y.; Cheng, G. M.; Weber, D.; Pielhofer, F.; Lei, S. M.; Klemenz, S.; Yeh, Y. W.; Filsinger, K. A.; Arnold, C. B.; Yao, N.; Schoop, L. M. Soft Chemical Synthesis of  $\text{H}_2\text{CrS}_2$ : An Antiferromagnetic Material with Alternating Amorphous and Crystalline Layers. *J. Am. Chem. Soc.* **2019**, *141* (39), 15634–15640.

(58) Djieutedjeu, H.; Lopez, J. S.; Lu, R. M.; Buchanan, B.; Zhou, X. Y.; Chi, H.; Ranmohotti, K. G. S.; Uher, C.; Poudeu, P. F. P. Charge Disproportionation Triggers Bipolar Doping in  $\text{FeSb}_{2-x}\text{Sn}_x\text{Se}_4$  Ferromagnetic Semiconductors, Enabling a Temperature-Induced Lifshitz Transition. *J. Am. Chem. Soc.* **2019**, *141* (23), 9249–9261.

(59) Djieutedjeu, H.; Poudeu, P. F. P.; Takas, N. J.; Makongo, J. P. A.; Rotaru, A.; Ranmohotti, K. G. S.; Anglin, C. J.; Spinu, L.; Wiley, J. B. Structural-Distortion-Driven Cooperative Magnetic and Semiconductor-to-Insulator Transitions in Ferromagnetic  $\text{FeSb}_2\text{Se}_4$ . *Angew. Chem., Int. Ed.* **2010**, *49* (51), 9977–9981.

(60) Djieutedjeu, H.; Makongo, J. P. A.; Rotaru, A.; Palasyuk, A.; Takas, N. J.; Zhou, X. Y.; Ranmohotti, K. G. S.; Spinu, L.; Uher, C.; Poudeu, P. F. P. Crystal Structure, Charge Transport, and Magnetic Properties of  $\text{MnSb}_2\text{Se}_4$ . *Eur. J. Inorg. Chem.* **2011**, *2011* (26), 3969–3977.

(61) Ranmohotti, K. G. S.; Djieutedjeu, H.; Poudeu, P. F. P. Chemical Manipulation of Magnetic Ordering in  $\text{Mn}_{1-x}\text{Sn}_x\text{Bi}_2\text{Se}_4$  Solid-Solutions. *J. Am. Chem. Soc.* **2012**, *134* (34), 14033–14042.

(62) Ranmohotti, K. G. S.; Djieutedjeu, H.; Lopez, J.; Page, A.; Haldolaarachchige, N.; Chi, H.; Sahoo, P.; Uher, C.; Young, D.; Poudeu, P. F. P. Coexistence of High-Tc Ferromagnetism and n-Type Electrical Conductivity in  $\text{FeBi}_2\text{Se}_4$ . *J. Am. Chem. Soc.* **2015**, *137* (12), 4274–4274.

(63) Kong, T.; Stolze, K.; Ni, D. R.; Kushwaha, S. K.; Cava, R. J. Anisotropic magnetic properties of the ferromagnetic semiconductor  $\text{CrSbSe}_3$ . *Phys. Rev. Mater.* **2018**, *2* (1), 014410.

(64) Odink, D. A.; Carreaux, V.; Payen, C.; Ouvrard, G. Synthesis and Structure of  $\text{CrSbSe}_3$  - a Pseudo-One-Dimensional Ferromagnet. *Chem. Mater.* **1993**, *5* (2), 237–240.

(65) O'Barr, R.; Schultz, S. Switching Field Studies of Individual Single Domain Ni Columns. *J. Appl. Phys.* **1997**, *81* (8), 5458–5460.

(66) Balan, A. P.; Radhakrishnan, S.; Woellner, C. F.; Sinha, S. K.; Deng, L. Z.; de los Reyes, C.; Rao, B. M.; Paulose, M.; Neupane, R.; Apte, A.; Kochat, V.; Vajtai, R.; Harutyunyan, A. R.; Chu, C. W.; Costin, G.; Galvao, D. S.; Marti, A. A.; van Aken, P. A.; Varghese, O. K.; Tiwary, C. S.; Iyer, A. M. M. R.; Ajayan, P. M. Exfoliation of a Non-van der Waals Material from Iron ore Hematite. *Nat. Nanotechnol.* **2018**, *13* (7), 602–609.

(67) Backes, C.; Higgins, T. M.; Kelly, A.; Boland, C.; Harvey, A.; Hanlon, D.; Coleman, J. N. Guidelines for Exfoliation, Characterization and Processing of Layered Materials Produced by Liquid Exfoliation. *Chem. Mater.* **2017**, *29* (1), 243–255.

(68) Shen, J. F.; He, Y. M.; Wu, J. J.; Gao, C. T.; Keyshar, K.; Zhang, X.; Yang, Y. C.; Ye, M. X.; Vajtai, R.; Lou, J.; Ajayan, P. M. Liquid Phase Exfoliation of Two-Dimensional Materials by Directly Probing and Matching Surface Tension Components. *Nano Lett.* **2015**, *15* (8), 5449–5454.

(69) Wang, M.; Xu, X. W.; Ge, Y. C.; Dong, P.; Baines, R.; Ajayan, P. M.; Ye, M. X.; Shen, J. F. Surface Tension Components Ratio: An Efficient Parameter for Direct Liquid Phase Exfoliation. *ACS Appl. Mater. Interfaces* **2017**, *9* (10), 9168–9175.

(70) Halim, U.; Zheng, C. R.; Chen, Y.; Lin, Z.; Jiang, S.; Cheng, R.; Huang, Y.; Duan, X. A Rational Design of Cosolvent Exfoliation of Layered Materials by Directly Probing Liquid-solid Interaction. *Nat. Commun.* **2013**, *4*, 2213.

(71) Shen, J. F.; Wu, J. J.; Wang, M.; Dong, P.; Xu, J. X.; Li, X. G.; Zhang, X.; Yuan, J. H.; Wang, X. F.; Ye, M. X.; Vajtai, R.; Lou, J.; Ajayan, P. M. Surface Tension Components Based Selection of Cosolvents for Efficient Liquid Phase Exfoliation of 2D Materials. *Small* **2016**, *12* (20), 2741–2749.

(72) Jia, X.; Lin, Z.; Zhang, T.; Puthen-Veetil, B.; Yang, T.; Nomoto, K.; Ding, J.; Conibeer, G.; Perez-Wurfl, I. Accurate Analysis of the Size Distribution and Crystallinity of Boron Doped Si Nanocrystals via Raman and PL spectra. *RSC Adv.* **2017**, *7* (54), 34244–34250.

(73) Ramaraj, S.; Mani, S.; Chen, S. M.; Palanisamy, S.; Velusamy, V.; Hall, J. M.; Chen, T. W.; Tseng, T. W. Hydrothermal Synthesis of  $\text{Cr}_2\text{Se}_3$  Hexagons for Sensitive and Low-level Detection of 4-Nitrophenol in Water. *Sci. Rep.* **2018**, *8*, 4839.

(74) Biesinger, M. C.; Payne, B. P.; Grosvenor, A. P.; Lau, L. W. M.; Gerson, A. R.; Smart, R. S. Resolving Surface Chemical States in XPS Analysis of First Row Transition Metals, Oxides and Hydroxides: Cr, Mn, Fe, Co and Ni. *Appl. Surf. Sci.* **2011**, *257* (7), 2717–2730.

(75) Liu, X. S.; Chen, J.; Luo, M.; Leng, M. Y.; Xia, Z.; Zhou, Y.; Qin, S. K.; Xue, D. J.; Lv, L.; Huang, H.; Niu, D. M.; Tang, J. Thermal Evaporation and Characterization of  $\text{Sb}_2\text{Se}_3$  Thin Film for Substrate  $\text{Sb}_2\text{Se}_3/\text{CdS}$  Solar Cells. *ACS Appl. Mater. Interfaces* **2014**, *6* (13), 10687–10695.

(76) Park, B. C.; Kim, Y. K. Synthesis, Microstructure, and Physical Properties of Metallic Barcode Nanowires. *Met. Mater. Int.* **2017**, *23* (3), 413–425.

(77) Sun, L.; Hao, Y.; Chien, C. L.; Searson, P. C. Tuning the Properties of Magnetic Nanowires. *IBM J. Res. Dev.* **2005**, *49* (1), 79–102.

(78) Pignard, S.; Goglio, G.; Radulescu, A.; Piroux, L.; Dubois, S.; Declémy, A.; Duvail, J. L. Study of the Magnetization Reversal in Individual Nickel Nanowires. *J. Appl. Phys.* **2000**, *87* (2), 824–829.

(79) Zhang, R. J.; Willis, R. F. Thickness-dependent Curie Temperatures of Ultrathin Magnetic Films: Effect of the Range of Spin-spin Interactions. *Phys. Rev. Lett.* **2001**, *86* (12), 2665–2668.

(80) Tan, C.; Lee, J.; Jung, S. G.; Park, T.; Albarakati, S.; Partridge, J.; Field, M. R.; McCulloch, D. G.; Wang, L.; Lee, C. Hard Magnetic Properties in Nanoflake van der Waals  $\text{Fe}_3\text{GeTe}_2$ . *Nat. Commun.* **2018**, *9*, 1554.

(81) Londono-Calderon, C. L.; Moscoso-Londono, O.; Muraca, D.; Arzuza, L.; Carvalho, P.; Pirola, K. R.; Knobel, M.; Pampillo, L. G.; Martinez-Garcia, R. Synthesis and Magnetic Properties of Cobalt-iron/cobalt-ferrite Soft/hard Magnetic Core/shell Nanowires. *Nanotechnology* **2017**, *28* (24), 245605.

(82) Schlorb, H.; Uhlemann, M.; Haehnel, V.; Iselt, D.; Gebert, A. Electrodeposition of Fe-based Magnetic Alloy Nanowires. *Z. Phys. Chem.* **2013**, *227* (8), 1071–1082.

(83) Yang, W.; Cui, C. X.; Sun, J. B.; Wang, B. L. Fabrication and Magnetic Properties of Fe<sub>3</sub>Co<sub>7</sub> Alloy Nanowire Arrays. *J. Mater. Sci.* **2010**, *45* (6), 1523–1527.

(84) Li, C. L.; Wu, Q.; Yue, M.; Xu, H. H.; Palaka, S.; Elkins, K.; Liu, J. P. Manipulation of Morphology and Magnetic Properties in Cobalt Nanowires. *AIP Adv.* **2017**, *7* (5), 056229.

(85) Tejada, J.; Zhang, X. X.; Hernandez, J. M. Magnetic Viscosity and Hysteresis Phenomena. In *Magnetic Hysteresis in Novel Magnetic Materials*; Hadjipanayis, G. C., Ed.; Springer: Dordrecht, The Netherlands, 1997; Vol. 338, pp 221–232.

(86) Kardar, M. *Statistical Physics of Fields*; Cambridge University Press, 2012.

(87) Tang, Z. X.; Sorensen, C. M.; Klabunde, K. J.; Hadjipanayis, G. C. Size-Dependent Curie-Temperature in Nanoscale MnFe<sub>2</sub>O<sub>4</sub> Particles. *Phys. Rev. Lett.* **1991**, *67* (25), 3602–3605.

(88) Koon, N. C.; Jonker, B. T.; Volkening, F. A.; Krebs, J. J.; Prinz, G. A. Direct Evidence for Perpendicular Spin Orientations and Enhanced Hyperfine Fields in Ultrathin Fe(100) Films on Ag(100). *Phys. Rev. Lett.* **1987**, *59* (21), 2463–2466.

(89) Childress, J. R.; Chien, C. L.; Jankowski, A. F. Magnetization, Curie-Temperature, and Magnetic-Anisotropy of Strained (111) Ni/Au Superlattices. *Phys. Rev. B: Condens. Matter Mater. Phys.* **1992**, *45* (6), 2855–2862.

(90) Li, Y.; Baberschke, K. Dimensional Crossover in Ultrathin Ni(111) Films on W(110). *Phys. Rev. Lett.* **1992**, *68* (8), 1208–1211.

(91) Lopez-Ruiz, R.; Magen, C.; Luis, F.; Bartolome, J. High Temperature Finite-size Effects in the Magnetic Properties of Ni Nanowires. *J. Appl. Phys.* **2012**, *112* (7), 073906.